ASTFE American Society of Thermal and Fluids Engineers

9th Thermal and Fluids Engineering Conference (TFEC)
April 21-24, 2024
Partially Online Virtual and at Oregon State University, OR Conference

TFEC-2024-50458

EFFECTS OF IMPELLER VANE COUNT AND CASING TYPE ON SLURRY PUMP PERFORMANCE INSTABILITY

Mohamed Garman[1]*, Brain Prochaska[1] and Robert Visintainer[1]

[1]GIW Industries, Inc., 5000 Wrightsboro Road, Grovetown, GA 30813

ABSTRACT

Centrifugal slurry pumps are designed for pumping a mixture of solids and liquids and are widely used in the mining and dredging industries. These pumps tend to be large and run at low pump speeds to increase wear life. Their design is different from that of clear liquid pumps, as slurry pumps must often pass large solids and require large flow passages to prevent blockages. This pump configuration can lead to a hydraulic mismatch between the casing and impeller or to hydraulic instability. In the current investigation, two impellers with four and six vanes, respectively, were used in two casing types, annular (AH) and semi-volute (CH), for a total of four combinations. The test results showed significant instability in the head curve when the AH casing was used. The instability persisted over a large portion of the curve, resulting in a much lower operating efficiency. In general, changing to the CH casing mitigated the instability and restored the expected pump efficiency. Changing from a four- to a six-vane impeller did not show a significant effect on the efficiency, but it did show a substantial impact on the head, especially with the CH casing type. To investigate the root cause of hydraulic instability, a high-fidelity, transient, full-machine model, including the impeller side gap, was developed and applied in a flow range from about 20% to 140% of the pump's best efficiency flow rate (Q_{BEP}). The simulation results agreed well with the measured performances, detecting the instability at the same flow rate for the AH casing type and no instability with the CH casing type. A considerable difference in the simulation results was found in the volute (close to the cutwater region) and within the impeller passages.

KEY WORDS: Slurry pump, hydraulic instability, CFD, high-fidelity transient simulation

NOMENCLATURE

AH	annular casing	
CH	semi-volute casing	
CFD	computational fluid mechanics	
D_2	impeller diameter	(m)
g	gravitational acceleration	(m/s^2)
H	total developed head	(m)
M	torque	(N-m)
n	pump speed	(rpm)
N_s	pump specific speed	(-)
P_{in}	power input	(W)
P_{out}	power output	(W)
Q	flow rate	(GPM)
Q_{BEP}	best efficiency flow rate	(GPM)
Q_D	design flow rate	(GPM)
R	radius ratio	(-)
TKE	turbulent kinetic energy	(J/kg)
r_2	impeller radius	(m)
r_3	radius (pump center to inside tongue)	(m)
r_{t3}	radius at theoretical throat	(m)
W_r	wrap ratio	(-)
η	efficiency	(%)
ρ	fluid density	(kg/m^3)
θ	throat-to-tongue angle	(degree)

*Corresponding Author: Mohamed.Garman@ksb.com

1. INTRODUCTION

Centrifugal slurry pumps are designed to handle two-phase flows (a mixture of solid and liquid). They tend to be large and run at low pump speed to increase the wear life. Slurry pumps often pass large solids, and a large sphere clearance is required in order to prevent blockages. This pump configuration can result in a hydraulic mismatch between the casing and the impeller, or in hydraulic instability.

Ye et al. [1] studied centrifugal pump instability analysis under part load conditions experimentally and numerically. They identified that the largest energy loss resulted from a strong reverse flow upstream of the impeller, which led to nearly complete impeller blockage. In an investigation of the losses for low–specific speed pumps, Juckelandt et al. [2] found that the main losses originated from the volute and the side gap.

Detailed particle image velocimetry (PIV) measurements by Wang et al. [3] showed substantial vortices within the impeller passage that led to a blockage. Measurements also showed that the size of the vortices was a function of the flow rate.

There are multiple reasons for energy loss that could influence hydraulic instability. In general, friction and flow separation are among the main causes of energy loss. The mixing of stalled fluid with the non-separated flows also contributes to a high energy loss [4]. Keller et al. [5] showed that the blade-tongue interaction is dominated by high vorticity and that the interaction is maximal when the blade aligns with the tongue tip. Recent studies have shown that a reduction in energy loss can be achieved by increasing the casing size, thereby reducing the fluid interaction level with the casing cutwater [6].

In the current investigation, two impellers with four and six vanes, respectively, were used in two casing types, annular (AH) and semi-volute (CH), for a total of four combinations. The test results showed significant instability in the head curve when the AH casing was used. This instability persisted over a large portion of the curve, resulting in a much lower operating efficiency. In general, changing to a CH casing mitigated the instability and restored the expected pump efficiency. Increasing the number of impeller vanes did not show a substantial effect on the efficiency close to best efficiency flow rate (Q_{BEP}) or higher flow, and it showed only a slight difference in the efficiency at low flows. However, increasing the number of vanes did show a significant impact on the head, especially with the CH casing.

To investigate the root cause of the hydraulic instability, a high-fidelity, transient, full-machine model, including the impeller side gap, was developed and applied in a flow range from about 20% to 140% Q_{BEP}. The simulation results agreed well with the measured performances, detecting the instability at the same flow rate with the AH casing and no instability with the CH casing. A considerable difference in the flow fields was found in the volute (close to the cutwater region) and within the impeller passages.
The naming convention throughout this paper will be as follows: 4ME-AH (4-vane impeller/AH casing); 4ME-CH (4-vane impeller/CH casing); 6ME-AH (6-vane impeller/AH casing), and 6ME-CH (6-vane impeller/CH casing).

*Corresponding Author: Mohamed.Garman@ksb.com

2. EXPERIMENTAL SETUP

The test loop (Fig. 1) consisted of the slurry pump, the electric motor, a torque and flow-rate measurement device, pressure sensors, and a large tank. The flow rate was measured by a 7.51" inner-diameter (ID) orifice-plate flow meter, the torque by a Lebow 10K and 20K in-lbs torque bars, and the pressure by Yokogawa type-4 differential pressure transducers. The pressure transducers were located at a distance double the pipe diameter from the discharge flange and the suction flange. The pump specific speed (N_s) for the pumps under investigation was about 21.5 and 23.5 for the CH and AH casing types, respectively. The geometric parameters for the two casings and impellers are as shown in Table 1 and Table 2, respectively. Fig. 2 shows the casings' main geometric parameters.

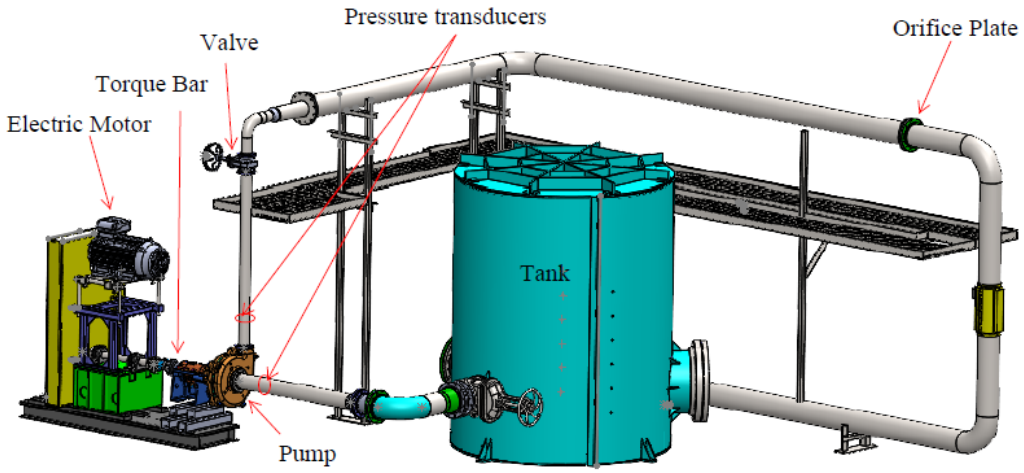

Fig. 1 Test loop

Table 1 Casings main geometric parameters

Parameters	CH Casing	AH Casing
Pump center to discharge face (mm)	482.6	558.8
Pump center to discharge center (mm)	450.9	355.6
Discharge diameter (mm)	152.4	
Inside shell width (mm)	158.8	
Radius to inside tongue (r_3) (mm)	395.2	438.2
Radius at theoretical throat (r_{t3}) (mm)	450.9	438.2
Tongue radius (mm)	31.8	39.6
Throat-to-tongue angle (θ) (degree)	47.5	57.5
W_r (-)	0.48	0
R (-)	1.19	1.35

Table 2 Impeller main geometric parameters

Parameters	4-Vane	6-Vane
Impeller vane diameter (D_2) (mm)	635	
Eye diameter (mm)	196.9	203.2
Impeller passage width (b_2) (mm)	92.1	
Vane inlet angle (degree)	32.21	30.5
Vane outlet angle (degree)	28	
Vane sweep angle (degree)	113.6	
Number of vanes	4	6

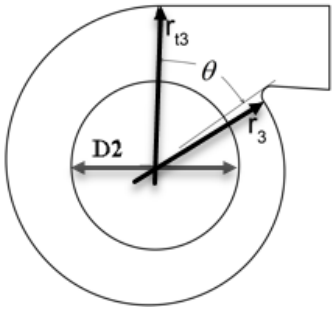

Fig. 2 Casing geometry

The definitions of wrap ratio (W_r) and the ratio (R) are shown in equations (1) and (2), respectively. A zero-value W_r represents an annular casing with no spiral, while a W_r value of unity represents a pure volute design configuration. The W_r and R for both casings are shown in Table 1. An earlier study [6] showed that when R is greater than one, a significant interaction with the casing's cutwater can be observed.

$$W_r = \frac{(r_{t3} - r_3)\frac{360}{360-\theta}}{(r_{t3} - r_2)} \tag{1}$$

$$R = \frac{r_2}{r_3 cos\theta} \tag{2}$$

where r_{t3} is the radius at theoretical throat, $r_2=D_2/2$ is the impeller radius, r_3 is the distance from the center of the pump to the inside tongue, and θ is the throat-to-tongue angle (Fig. 2.)

3. NUMERICAL MODEL

The implicit unsteady Reynolds-averaged Navier-Stokes (RANS) equations were used with a K-omega SST turbulence model and curvature correction. A rigid body motion was implemented, which moved the mesh vertices and cells during transient simulation [7].

The boundary conditions were as follows: at the inlet, mass flow inlet with 0.02 turbulent intensity; at the outlet, the mass flow rate leaving the boundary was specified based on the inflow mass flow rate, and the velocity and static pressure were extrapolated from the adjacent cell.

Smooth wall surfaces with no-slip boundary conditions were applied for all walls. The time step for all simulations was 60/(rpm*360) = 2.78E-04 sec (the time taken to rotate 1°). This time step was linearly ramped up over 20 time steps.

A polyhedral mesh, enhanced by a prism-layer mesher, was selected (16 prism layers for the impeller and 12 prism layers elsewhere). The base size for the automated mesh was 0.02 m. The thickness of the prism layer (for the impeller), which was near to the wall, was about 1E-5 m.

Fig. 3 shows the unstructured polyhedral mesh utilized in the current study for all pumps. The total number of cells and the percentage of cells for each part is shown in Table 3 for all pumps.

Impeller/Casing Combination	AH	CH
4ME		
6ME		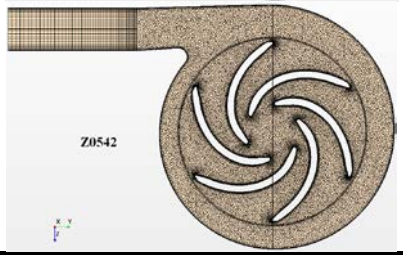

Fig. 3 Unstructured polyhedral mesh utilized in the current study

Table 3 Number of cells

Impeller/Casing Combination	Total # cells	Impeller (%)	Nose gap (%)	Casing (%)	Discharge pipe (%)	Suction pipe (%)
4ME-AH	9,576,493	60.3	15.9	12.9	0.6	10.3
4ME-CH	10,560723	61.7	17.0	11.3	0.5	9.4
6ME-AH	12,088,197	67.0	16.2	8.2	0.4	8.2
6ME-CH	13,394,653	64.4	14.2	13.7	0.4	7.3

The commercial software STAR-CCM+, version 2020.3, was used to run a high-fidelity, transient, full-machine model, including the impeller side gap, for a flow range of 1.7 to 0.25 Q_D (Q_D=2026 gpm) at 600 rpm for all pumps. The simulations ran for 20 impeller rotations, and the performance results were averaged over the last 10 impeller rotations of the simulations (about 40 and 60 vane passes for the four- and six-vane impellers, respectively). In general, the y+ values were typically less than 10 for the impeller and the casing.

The numerical simulation was used to study and analyze the flow field in order to determine an explanation for these kinds of performance instabilities. The measured head and efficiency for the four pump combinations are shown in Figs. 4 and 5, respectively.

In general, for the CH casing, the number of vanes did not have any significant effect on the efficiency, but an increase in vanes did show a substantial effect on head. For the AH casing, a significant effect on the efficiency for flow-rate ranges from 50 to 100% Q_D was observed. The four-vane impeller was able to mitigate this problem partially when it was used with the AH casing at low flow rates, as shown in Fig. 5.

A drop in the head resulted when going from the CH casing to the AH casing, as shown in Fig. 4. This drop resulted in an efficiency drop of about 10 points, as shown in Fig. 5.

The calculated head and efficiency for all pumps are shown in Figs. 6 and 7, respectively. The simulations were able to predict the performance curve similar to the actual testing. The simulation results showed a performance instability when an AH casing was used, and no instability when a CH casing was used.

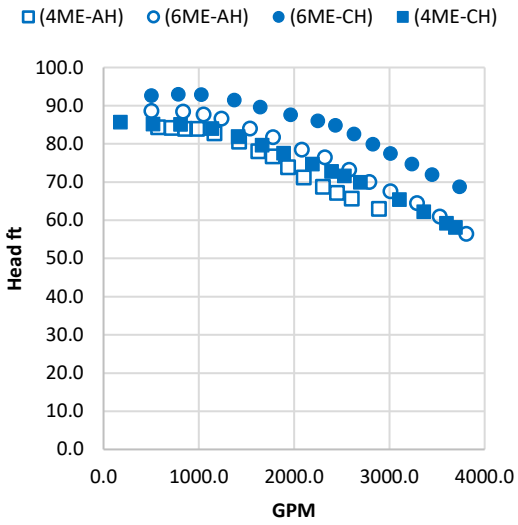

Fig. 4 Measured head

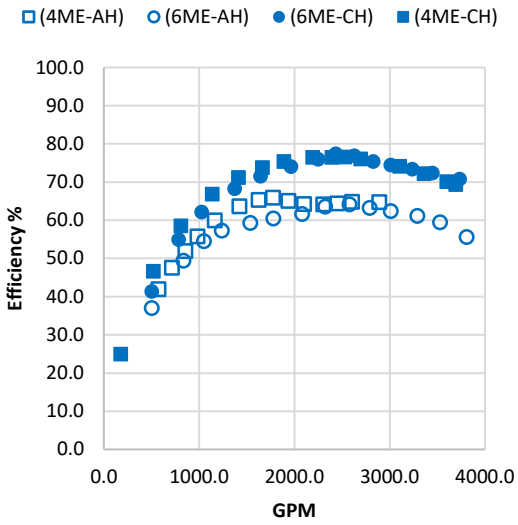

Fig. 5 Measured efficiency

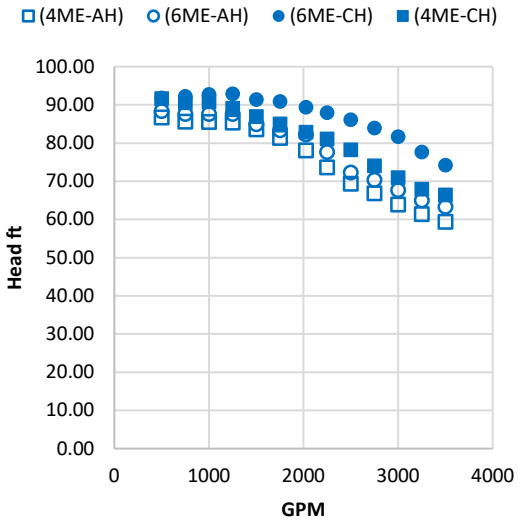

Fig. 6 Calculated head

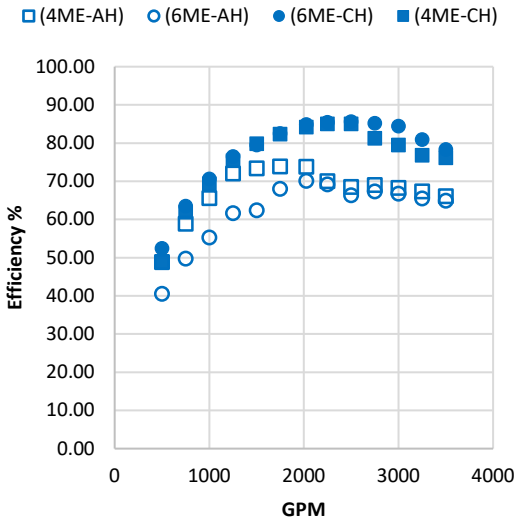

Fig. 7 Calculated efficiency

As Figs. 4 and 6 show, the calculated head and the measured head were almost identical for all impeller-casing combinations. The magnitude of the calculated efficiency was higher than the measured value by approximately eight percentage points. A significant portion of this loss was due to the wall roughness (the current study assumed smooth wall surfaces) [2]. By employing the W. K. Jekat equation [8] for the hydraulic loss as a function of flow rate $(1\text{-}0.8/[Q(GPM)]^{0.25})$, the estimated and the calculated performances were within the same order of magnitude. An examination of the aforementioned results (Figs. 4 to 7) indicates that the proposed CFD models are reliable and acceptable for the current analysis.

4. RESULTS AND DISCUSSION

This section will provide both the main differences of the flow field patterns obtained by the transient CFD simulations and the main causes of hydraulic instability.
Mixing loss was considered one of the main causes of energy loss [4]. The difference between the input (P_{in}) and output (P_{out}) power will represent the energy loss or the loss in power, calculated as follows:

$$P_{in} = 2\pi nM/60 \tag{3}$$

$$P_{out} = \rho gHQ \tag{4}$$

where $\rho, g, H, Q, n,$ and M are fluid density, gravitational acceleration, total developed head, volume flow rate, pump speed, and the torque, respectively.

The torque from the CFD simulation was calculated by integrating the pressure and the shear stresses exerted on the impeller, including the clearing vanes situated in the side gap.

Fig. 8 shows the loss in power for all pumps. The casing type had a significant effect on the power loss. When the CH casing was in use, the power loss had a minimum value close to its % Q_{BEP}, and it was increased away from the % Q_{BEP}. On the other hand, when the AH casing was in use, the loss in power was very high, and then it decreased by decreasing the flow rate up to a flow close to its % Q_{BEP}. Lowering the flow rate to a value lower than the % Q_{BEP} did not show a significant effect on the power loss. In all events, the CH casing design helped to mitigate the performance-instability problem.
When the CH casing was in use, the number of vanes did not show a substantial effect on the power loss. On the other hand, when the AH casing was in use, a significant effect on the power loss was observed. At lower flow rates, a higher number of vanes produced a greater power loss, as shown in Fig. 8.

The torque generally increased by increasing the flow rate, as shown in Fig. 9. The 6ME-AH had the highest torque at all flow rates, which explains why this combination had the lowest efficiency compared to the remainder. All of other pump combinations had similar torque at low flow rates, and the torque changed slightly at the Q_{BEP} and higher.

In Fig. 10, the relative tangential velocity shows a location within the AH casing where flow was significantly disturbed. Those areas were close to the cutwater and downstream of the cutwater region. The flow interaction with the cutwater area had a significant effect on reducing the performance in term of mixing losses. These areas of disturbed flow were not significant when the CH casing was used. In general, the casing type dominates the mixing loss despite the impellers vane count. The semi-volute (CH) casing, with smaller R and larger W_r, were the reasons in mitigating the instability problem.

One way to visualize the mixing loss is by calculating and visualizing the fluid volume in terms of TKE (turbulent kinetic energy, J/kg), which considers the kinetic energy per unit mass as an outcome of the eddies in the turbulent flow. Equation (5) shows the equation used to calculate the TKE.

$$\mathrm{TKE} = \frac{1}{2}(\overline{\acute{u}^2} + \overline{\acute{v}^2} + \overline{\acute{w}^2}) \tag{5}$$

where $\acute{u}, \acute{v},$ and $\acute{w}$ are the difference between the instantaneous and average velocities for each velocity component.

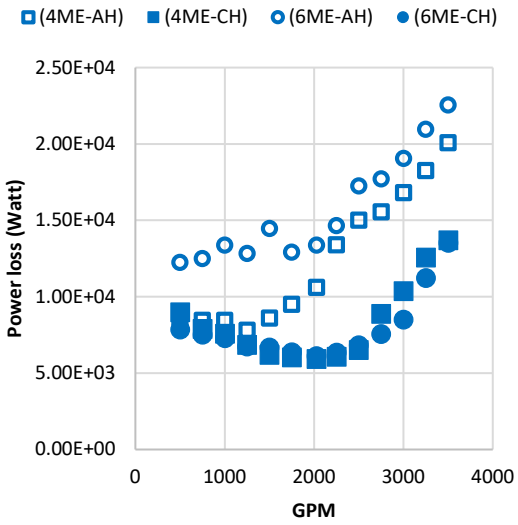

Fig. 8: Power loss

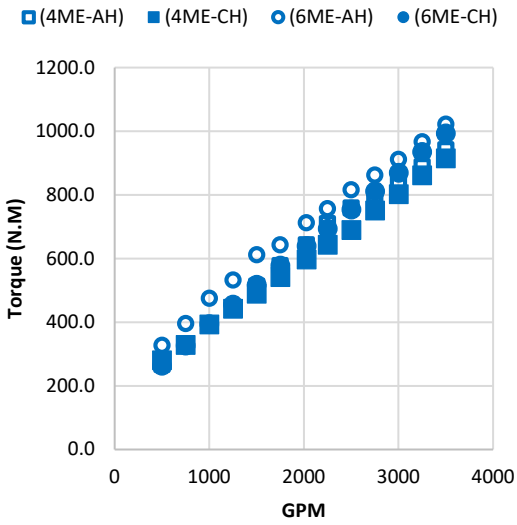

Fig. 9: Calculated torque

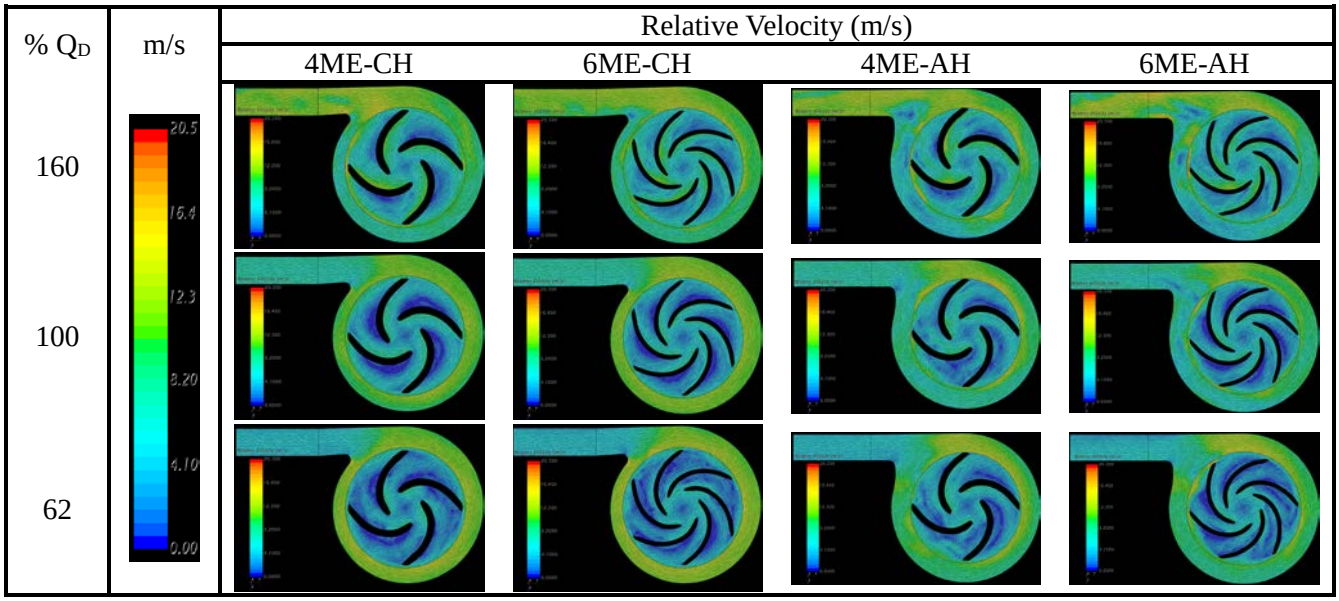

Fig. 10 Relative tangential velocity

Fig. 11 shows the TKE for all pumps. Fig. 11 supports Fig. 10 in showing the location of high turbulent intensity at the same zones of the disturbed flow, which led to a loss in performance in terms of mixing loss. There was no significant mixing loss when the CH casing was uses, but there was a significant mixing loss in the region close to the cutwater and downstream of the cutwater area when the AH casing was uses. The ratio (*R*) shown in this study was larger for AH casing as compared to CH casing, and, according to the TKE results, the AH casing (large *R*) was occupied by a large zone of high TKE close to the tongue region. This kind of turbulent intensity will cause high degree of loss in power because of the mixing effect. These areas of high intensity became smaller and less intense as flow rate decreased. Fig. 11 also shows that the region of high turbulent intensity (mixing loss) at a high flow rate was dominated by the interaction with the cutwater, whereas at low flow, the mixing loss was dominated by the interaction with the vane trailing edge.

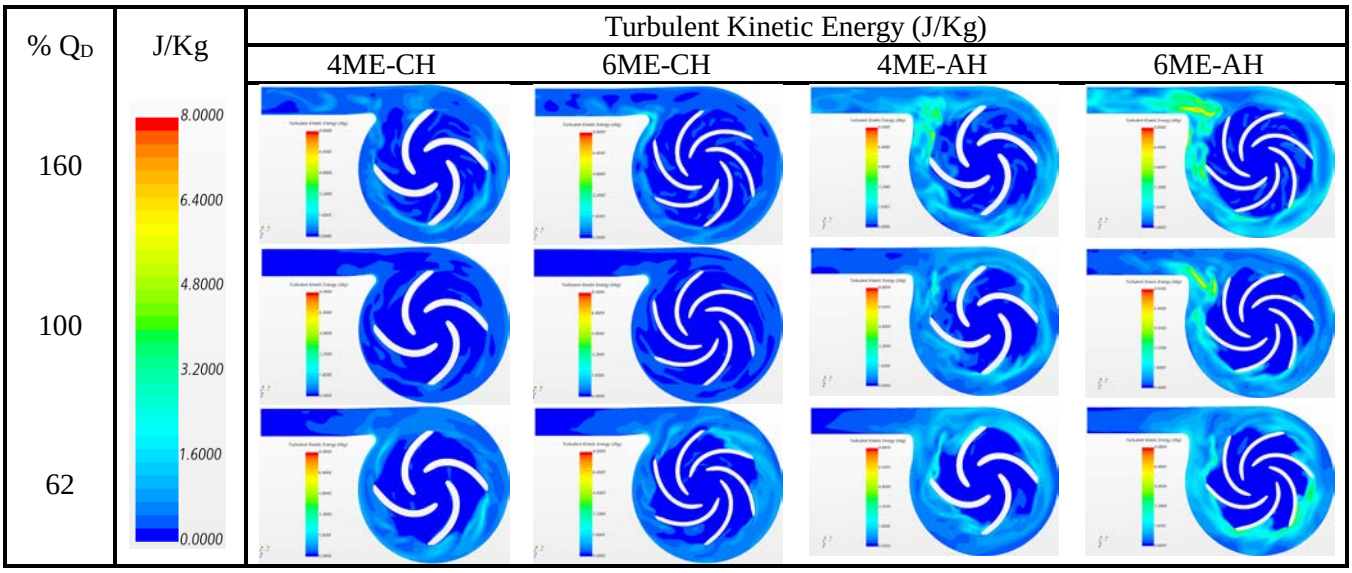

Fig. 11 Turbulent kinetic energy

Fig. 12 shows the volume (percentage relative to the pump fluid volume) associated with those high-turbulent-intensity locations that have been summed for each pump for all turbulent intensities greater than 3 J/kg and for all flow rates. Fig. 12 clearly shows that the AH casing had a high level of mixing loss at a high flow rate. The 4-vane impeller may have mitigated some of these mixing losses since fewer vanes were interacting with the flow within the pump casing.

The area close to the cutwater for the AH casing was larger compared to that of the CH casing. In addition to the larger *R*, the interaction level of the flow with the cutwater was amplified. This interaction propagated to fluid zones downstream of the cutwater and back toward the casing. As a result, the fluid flow was significantly disturbed. This disturbance was the main reason for the mixing loss and the observed instability at high flow rates for the AH casing.

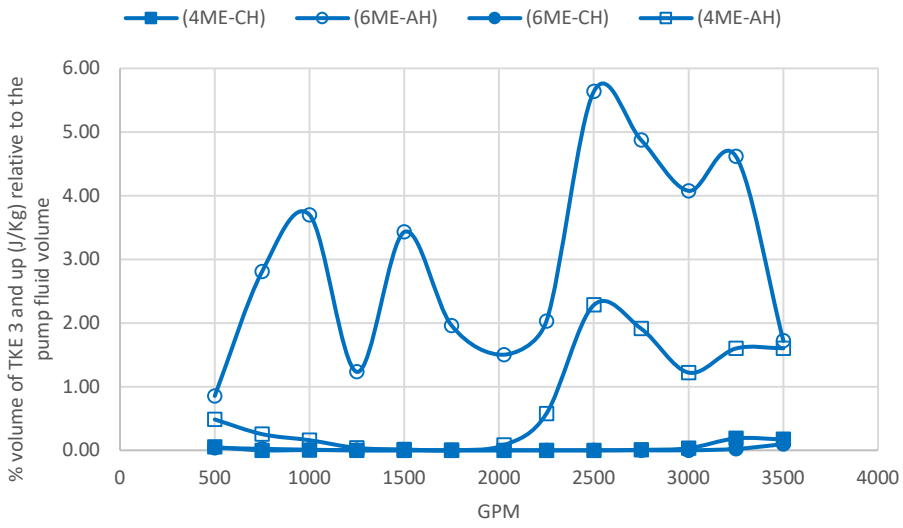

Fig. 12 % Volume of turbulent kinetic energy (>3 J/kg)

5. CONCLUSIONS

The phenomenon of hydraulic instability was investigated by using a high-fidelity, transient, full-machine model to analyze flow patterns and determine the root cause. CFD simulation results showed a good agreement with the measured performances. The observed (from the CFD) instability was detected at the same flow rate (from the measured) when utilizing the AH casing. From the current analysis, the following conclusions can be drawn:

- The developed numerical treatment is suitable for the simulation of hydraulic instability and its remedy.
- The mixing loss was the main cause of the hydraulic instability.
- The reduction of *R* ratio may have mitigated some of the performance instability.
- In the case of the CH casing, the number of vanes did not have any significant effect on the efficiency, but an increase in the number of vanes showed a substantial effect on head.
- In the case of the AH casing, the number of vanes did not play an important role for the hydraulic instability at high flow rates.
- At low flow rates, as with the AH casing, a greater number of vanes increased the interaction level of the flow with the trailing edge of the impeller. This resulted in a higher power loss (mixing loss) and a noticeable drop in the efficiency.
- The area close to the cutwater for the AH casing is larger compared to the CH casing. In addition to the larger *R* ratio, the interaction level between the flow and the cutwater region was increased. The propagation of this interaction to the area downstream of the cutwater and back toward the casing was the main reason of disturbing the flow within the casing domain. This led to an energy loss that was felt by the pump as a hydraulic instability at high flow rate when utilizing the AH casing.
- In general, the casing type dominates the mixing loss despite the impeller's vane count. The semi-volute (CH) casing, with smaller R and larger W_r, was the reason behind mitigating the hydraulic instability problem.
- At high flow rates in the AH casing, the loss in power was dominated by the flow interaction with the cutwater, while at low flow, the loss in power was dominated by the flow interaction with the vane trailing edge.

ACKNOWLEDGMENTS

The authors gratefully acknowledge the help of all the personnel involved in this study, and they especially acknowledge the outstanding contribution of the Hydraulic Lab at GIW Industries, Grovetown, Georgia, in developing and installing the test rig, and in conducting the necessary testing for the current study. The authors also acknowledge the following people for their help: Mr. Chad Thompson for creating 3D fluid models that were crucial input to the CFD simulations; Mrs. Janina Rogers, Mr. Travis Basinger, Mr. Riley Carlson, and Miss Eylaaf Garman for reviewing the content and the manuscript of the paper; and Mr. Edwin Thompson for creating the 3D test rig model.

REFERENCES

[1] Weixiang Ye, Renfang Huang, Zhiwu Jiang, Xiaojun Li, Zuchao Zhu and Xianwu Luo, Instability analysis under part-load conditions in centrifugal pump, Journal of Mechanical Science and Technology 33 (1) (2019) 1~10.

[2] K. Juckelandt - S. Bleeck - F.-H. Wurm, Analysis Of Losses In Centrifugal Pumps With Low Specific Speed With Smooth And Rough Walls, Proceedings of 11th European Conference on Turbomachinery Fluid dynamics & Thermodynamics ETC11, March 23-27, 2015, Madrid, Spain.

[3] Yanping Wang, Hui Yang, Bo Chen, Panlong Gao, Hui Chen, Zuchao Zhu, Analysis of vortices formed in flow passage of a five-bladed centrifugal water pump by means of PIV method, AIP Advances 9, 075011 (2019), https://doi.org/10.1063/1.5099530.

[4] Johann Friedrich Gülich, Centrifugal Pumps, Second edition, Springer, 2010.

[5] Jens Keller, Eduardo Blanco, Raúl Barrio, Jorge Parrondo, PIV measurements of the unsteady flow structures in a volute centrifugal pump at a high flow rate, Experiments in Fluids volume 55, Article number: 1820 (2014). https://doi.org/10.1007/s00348-014-1820-7

[6] Mohamed Garman and Robert Visintainer, Slurry Pumps Instability Investigation Using High Fidelity CFD Simulation, Proceedings of the ASME 2022 Fluids Engineering Division Summer Meeting FEDSM2022 August 3-5, 2022, Toronto, Ontario, Canada.

[7] Simcenter STAR-CCM+ Documentation, Version 2020.3.

[8] Igor J. Karassik, Joseph P. Messina, Paul Cooper, Charles C. Heald, Pump Handbook, Third Edition, McGraw-Hill, 2001.